CFD Letters www.cfdl.issres.net Vol. 5 (3) – September 2013

Simulation of Incompressible Flow in Two Sided Lid Driven Cavity using Upwind Compact Scheme

A. Munir[2], M. Rizwan[1], M. Khan[2] , A.Shah[1*]

[1]*Department of Mathematics, COMSATS Institute of Information Technology, Park Road Islamabad, Pakistan.*
[2]*Department of Mathematics, Quaid-i-Azam University, Islamabad, Pakistan.*

Received: 23/04/2012 – Revised 21/06/2013 – Accepted 25/06/2013

Abstract

In this paper, the flow inside the two sided lid driven cavity is simulated using third order upwind compact finite difference scheme based on flux difference splitting in combination with artificial compressibility approach. The results are compared with alternate direction implicit finite difference scheme. Unlike single lid driven cavity, there is free shear layer and two symmetric secondary eddies growing in size directly with Reynolds numbers for parallel wall motion. However, for anti parallel wall motion the eddy structure changes, the secondary eddies appear in upper left and lower right corners.

Keywords: two-sided lid-driven square cavity; artificial compressibility method; third order upwind compact scheme; parallel wall motion; anti parallel wall motion

1. Introduction

With the rapid development of computational techniques and availability of high speed computers, there has been a continuously widening scope of scientific and engineering problems that can be solved numerically. A proper mathematical model and a good numerical scheme can provide realistic answers to complex physical phenomena for which analytical solution has not available. Most of the modelled partial differential equations (PDE's) for science and engineering problems do not possess the exact solutions, so we have to refer to numerical solution of these differential equations. As computer technology progressed, a computational approach became viable to deal with increasingly complicated flow problems. A desirable attribute of the computational fluid dynamics (CFD) technique is its flexibility when conducting parametric studies. Increasing interest in numerical computing demanding high accuracy for a wide range of scientific and engineering problems, therefore efficient and high resolution schemes become a major challenge to numerical scientists. Particularly

* Corresponding Author: Abdullah Shah
Email: scholar.cm@gmail.com Telephone: +0092 321 5022236
 PII: S2180-1363(13)5357-X

locally high-order finite difference, finite-volume and finite element methods have received more attention than traditional globally high-order methods such as spectral methods [1, 2] because the former are more robust in handling problems with complicated geometries than the latter. Compact finite difference schemes [3, 4] provide an effective way of combing the robustness of the finite difference schemes and the accuracy of spectral methods. Generally, in compact finite differences the computation of derivatives is implicit in the sense that derivative values at a particular node are computed not only from the function values but also from the values of the derivative at the neighbouring nodes. Compared to non-compact schemes of the same order of accuracy, compact schemes utilize a smaller stencil, have smaller truncating errors, and give better resolution. Compact finite difference scheme are classified into two main categories: central and upwind compact schemes. Central compact schemes have the advantage of achieving higher order accuracy with fewer grid points in the stencil, but have non-dissipative nature. Therefore, using central compact schemes on non-staggered grids for convective terms may cause numerical oscillations even for flows without discontinuities. On the other hand, upwind compact schemes with dissipative properties are more stable than central compact schemes. Fu and Ma [5, 6] among others [7-9] have developed some upwind compact schemes. As these upwind compact schemes can automatically provide grid-scale linkage for each variable to avoid odd-even decoupling and appropriate dissipation to prevent non-physical oscillations, they seem to be more suitable for discretizing the convective terms. This will make it easier to develop solution methods capable of handling problems with complicated geometries. The numerical method developed in [9] is tested in solving two sided moving lid driven cavity and the computed results are compared with those obtained in [10,14] using finite difference method. The comparison of the two schemes agrees very well.

The flow in cavity driven by a moving side walls is of basic importance for the study of vortex flows in closed geometries. Moreover, it is related to many engineering applications such as the flow over structures in airfoils, the cooling flow over electronic devices, or in the flow in short dwell coaters. Ghia et al. [10] have applied a multi grid method and given solutions for Reynolds numbers ranging from 100 to as high as 10000. Kuhlmann and others [11-12] have investigated two sided lid driven cavity with various span wise aspect ratios. They explored the nonlinear regime and found multiple two dimensional states in rectangular cavities. They also found seven and five flow states in anti-parallel and parallel motion respectively. Blohm and Kuhlmann [13] experimentally investigated the incompressible fluid flow in a rectangular container driven by two facing sidewalls which move steadily in an anti-parallel direction up to Re = 1200. D. A Perumal et al. [14] simulated incompressible flows in two sided lid driven square cavity by finite difference method.
The present work is concerned with the computation of two-sided lid-driven square cavity flows by using the numerical scheme developed by A. Shah and Li Yuan [9].

This rest of the paper is organized as follows. In Section 2, the formulation of the governing equations with artificial compressibility (AC) term is briefly outlined. In Section 3, the code is validated with benchmark results. Section 4 contains the numerical results. Pressure and vorticity fields in square cavity are briefly discussed in Section 5 and concluding remarks are made in Section 6.

2. Governing Equations

The governing equations are the non-dimensional incompressible Navier-Stokes equations in Cartesian coordinates (x, y) in conservative form and with the artificial term added to continuity and momentum equations using pseudo time approaches:

$$\frac{\partial \mathbf{Q}}{\partial ²} + \frac{\partial(\mathbf{E} - \mathbf{E}_v)}{\partial x} + \frac{\partial(\mathbf{F} - \mathbf{F}_v)}{\partial y} = \mathbf{0} \quad (1)$$

with

$$\mathbf{Q} = \begin{pmatrix} p \\ u \\ v \end{pmatrix}, \mathbf{E} = \begin{pmatrix} u \\ u^2 + p \\ uv \end{pmatrix}, \mathbf{F} = \begin{pmatrix} v \\ uv \\ v^2 + p \end{pmatrix}, \mathbf{E}_v = \frac{1}{\mathrm{Re}} \begin{pmatrix} 0 \\ u_x \\ v_x \end{pmatrix}, \mathbf{F}_v = \frac{1}{\mathrm{Re}} \begin{pmatrix} 0 \\ u_y \\ v_y \end{pmatrix}.$$

Here $\mathbf{Q}$ is the solution vector, $²$ is the pseudo-time or an iterative parameter, u and v are the velocity components, p is the pressure, Re is the Reynolds number, $\mathbf{I}_m$ is the modified identity matrix and is the artificial compressibility factor whose value is very important for the stability and convergence of the method. The $\mathbf{E}$ and $\mathbf{F}$ are the inviscid flux vectors while $\mathbf{E}_v$ and $\mathbf{F}_v$ are the viscous flux vectors in x and y directions respectively. The Jacobian matrices $\mathbf{A}$ and $\mathbf{B}$ of the inviscid flux vectors are

$$\mathbf{A} = \frac{\partial \mathbf{E}}{\partial \mathbf{Q}} = \begin{bmatrix} 0 & & 0 \\ 1 & 2u & 0 \\ 0 & v & u \end{bmatrix}, \ \mathbf{B} = \frac{\partial \mathbf{F}}{\partial \mathbf{Q}} = \begin{bmatrix} 0 & 0 & \\ 0 & v & u \\ 1 & 0 & v \end{bmatrix}$$

The Jacobian matrices $\mathbf{A}_v$ and $\mathbf{B}_v$ of the viscous flux vectors are

$$\mathbf{A}_v = \frac{\partial \mathbf{E}_v}{\partial \mathbf{Q}} = \frac{I_m}{\mathrm{Re}} \frac{\partial}{\partial x}, \ \mathbf{B}_v = \frac{I_m}{\mathrm{Re}} \frac{\partial}{\partial y} \text{ with } \mathbf{I}_m = \begin{bmatrix} 0 & 0 & 0 \\ 0 & 1 & 0 \\ 0 & 0 & 1 \end{bmatrix}$$

To get tri-diagonal system, matrices **A** and **B** are diagonalize as

$$\mathbf{A} = \mathbf{X}\mathbf{\Lambda}_\mathbf{A}\mathbf{X}^{-1}, \mathbf{B} = \mathbf{Y}\mathbf{\Lambda}_\mathbf{B}\mathbf{Y}^{-1} \quad (2)$$

where the diagonal matrices $\mathbf{\Lambda}_A$ and $\mathbf{\Lambda}_B$ contains the eigenvalues of matrices **A** and **B** respectively. **X** and **Y** are the matrices of the right eigenvectors, while $\mathbf{X}^{-1}$ and $\mathbf{Y}^{-1}$ are their inverses respectively.

3. Spatial Discretization

Since the governing equation are hyperbolic in nature, therefore the convective flux and its derivatives are split into two parts i.e., in the x direction

$$\mathbf{E}_x = \mathbf{E}^+{}_x + \mathbf{E}^-{}_x \quad (3)$$

These split derivatives can be computed using the following 3rd –order scheme

$$\frac{2}{3}\left(\mathbf{E}^+{}_x\right)_i + \frac{1}{3}\left(\mathbf{E}^+{}_x\right)_{i-1} = \frac{5¢^-\mathbf{E}^+{}_i + ¢^-\mathbf{E}^+{}_{i+1}}{6\Delta x} \quad (4a)$$

$$\frac{2}{3}\left(\mathbf{E}^-{}_x\right)_i + \frac{1}{3}\left(\mathbf{E}^-{}_x\right)_{i+1} = \frac{5¢^+\mathbf{E}^-{}_i + ¢^+\mathbf{E}^-{}_{i-1}}{6\Delta x} \quad (4b)$$

where $¢^+ f_i = f_{i+1} - f_i, ¢^- f_i = f_i - f_{i-1}$, and Δx is the grid spacing. The advantage of these upwind compact schemes is:

(1) their computational cost is small, as Eqs. (4) are explicitly marched forward and backward to get all the derivatives once the right-hand side (RHS) and the boundary derivatives are given;

(2) unlike central compact scheme, they provide odd-even coupling of grid points and numerical dissipation to damp out high-frequency oscillation; and

(3) they have better resolution properties than non-compact, upwind biased scheme of the

same order. Since each of the term in the RHS of Eqs.(4) represents the difference of split fluxes between neighboring points; one can compute them by using FDS [4]

$$\mathbf{E}^{\pm}{}_{i+1} - \mathbf{E}^{\pm}{}_{i} \equiv \Delta\mathbf{E}^{\pm}{}_{i+\frac{1}{2}} = \mathbf{A}^{\pm}(\overline{\mathbf{Q}})(\mathbf{Q}_{i+1} - \mathbf{Q}_{i})$$

where $\Delta E^{\pm}{}_{i+\frac{1}{2}}$ is the flux difference across the positive or negative traveling waves.

The split Jacobian matrix is calculated by $\mathbf{A}^{\pm}(\mathbf{Q}) = \mathbf{X}\,\mathbf{\Lambda}^{\pm}{}_{A}\mathbf{X}^{-1}$, which is evaluated using some intermediate value $\overline{\mathbf{Q}}$. The Roe properties [3], which are necessary for a conservative scheme, are satisfied exactly if $\overline{\mathbf{Q}}$ is taken as the average of the surrounding points, i.e.,

$$\overline{\mathbf{Q}} = \frac{1}{2}\left(\mathbf{Q}_{i+1} + \mathbf{Q}_{i}\right) . \tag{5}$$

To close the third order scheme, Eq. (4), at interior points, an explicit, dissipative, and third-order one-sided boundary scheme [5] is used at boundary grid points:

$$i = 1: \left(\mathbf{E}^{+}{}_{x}\right)_{i} = \frac{-11\mathbf{E}^{+}{}_{i} + 18\mathbf{E}^{+}{}_{i+1} - 9\mathbf{E}^{+}{}_{i+2} + 2\mathbf{E}^{+}{}_{i+3}}{6\Delta x}$$

$$= \frac{11\Delta\mathbf{E}^{+}{}_{i+\frac{1}{2}} - 7\Delta\mathbf{E}^{+}{}_{i+\frac{3}{2}} + 2\Delta\mathbf{E}^{+}{}_{i+\frac{5}{2}}}{6\Delta x} + O(\Delta x^{3}) \tag{6a}$$

$$i = N: \left(\mathbf{E}^{-}{}_{x}\right)_{i} = \frac{11\mathbf{E}^{-}{}_{i} - 18\mathbf{E}^{-}{}_{i-1} + 9\mathbf{E}^{-}{}_{i-2} - 2\mathbf{E}^{-}{}_{i-3}}{6\Delta x}$$

$$= \frac{11\Delta\mathbf{E}^{-}{}_{i-\frac{1}{2}} - 7\Delta\mathbf{E}^{-}{}_{i-\frac{3}{2}} + 2\Delta\mathbf{E}^{-}{}_{i-\frac{5}{2}}}{6\Delta x} + O(\Delta x^{3}) \tag{6b}$$

The discretization of the viscous terms is performed with central schemes because the viscous diffusion occurs in all directions. The second derivative for the viscous terms in Eq. (1) is approximated by a fourth-order symmetric compact scheme at the interior points

$$\frac{1}{12}\left(S_{i-1} + 10S_{i} + S_{i+1}\right) = \frac{u_{i-1} - 2u_{i} + u_{i+1}}{\Delta x^{2}}, \quad 2 \le i \le N-1 \tag{7}$$

where S_i approximate $\left(\dfrac{\partial^2 u}{\partial x^2}\right)_i$.

4. Implicit Approximate Factorization Scheme

By applying backward Euler difference scheme to the pseudo-time derivative, and three points, second-order backward difference scheme to the physical time derivative, one obtains

$$\frac{\Delta\mathbf{Q}^{m}}{\Delta^{2}} + \left[\frac{\partial\left(\mathbf{E} - \mathbf{E}_{v}\right)}{\partial x} + \frac{\partial\left(\mathbf{F} - \mathbf{F}_{v}\right)}{\partial y}\right]^{m+1} = \mathbf{0} \tag{8}$$

where $\Delta\mathbf{Q}^{m} = \mathbf{Q}^{m+1} - \mathbf{Q}^{m}$, the superscript n is the physical time level, and m is the pseudo time level. Δ^2 is the pseudo time step which is determined based on the CFL number and the superscript m is the pseudo time level. The residual term at *m+1* pseudo time level are linearized with respect to the previous time level *m* by using Taylor's expansion, i.e.,

$$\mathbf{E}^{m+1} \approx \mathbf{E}^{m} + \left(\frac{\partial\mathbf{E}}{\partial\mathbf{Q}}\right)^{m}\left(\mathbf{Q}^{m+1} - \mathbf{Q}^{m}\right) = \mathbf{E}^{m} + \mathbf{A}^{m}\Delta\mathbf{Q}^{m} \quad . \tag{9}$$

Thus obtains the unfactored implicit delta form as

$$\left[\mathbf{I}+\Delta^2\left(\frac{\partial(\mathbf{A}-\mathbf{A}_v)}{\partial x}+\frac{\partial(\mathbf{B}-\mathbf{B}_v)}{\partial y}\right)\right]^m \Delta\mathbf{Q}^m = -\Delta^2\left(\frac{\partial(\mathbf{E}-\mathbf{E}_v)}{\partial x}+\frac{\partial(\mathbf{F}-\mathbf{F}_v)}{\partial y}\right)^m = \mathbf{S}^m \qquad (10)$$

The equations are marched in pseudo time until R.H.S converges to zero. The Beam-Warming approximate factorization (AF) scheme can be symbolically written as

$£.\Delta\mathbf{Q}^{\mathrm{m}} \approx £_{\mathrm{x}}£_{\mathrm{y}}.\Delta\mathbf{Q}^{\mathrm{m}} = \mathbf{S}^{\mathrm{m}}.$

To obtain block tri-diagonal equations, convective terms in L.H.S of Eq. (10) are discretized by first order upwind difference and viscous terms by central difference, e.g.,

$$¢_x^{+} f_i = \frac{f_{i+1}-f_i}{\Delta x}, \quad ¢_x^{-} f_i = \frac{f_i - f_{i-1}}{\Delta x}, \quad ¢_x^{2} f_i = \frac{f_{i+1}-2f+f_{i-1}}{\Delta x^2}.$$

Remember that the upwind compact scheme is used for terms in the RHS $\mathbf{S}^m$. Thus, obtain the following form

$$\left[\mathbf{I}+\Delta^2\left(¢^{-}{}_x\mathbf{A}^{+}+¢^{-}{}_x\mathbf{A}^{-}-¢_x\mathbf{A}_v\right)+\Delta^2\left(¢^{-}{}_y\mathbf{B}^{+}+¢^{-}{}_y\mathbf{B}^{-}-¢_y\mathbf{B}_v\right)\right]^m\Delta\mathbf{Q}^m=\mathbf{S}^m.$$

Using similarity transformation of **A** and **B**, we have

$$\left[\mathbf{I}+\Delta^2\left(¢^{-}{}_x\mathbf{X}\mathbf{\Lambda}^{+}{}_{\mathbf{A}}\mathbf{X}^{-1}+¢^{+}{}_x\mathbf{X}\mathbf{\Lambda}^{-}{}_{\mathbf{A}}\mathbf{X}^{-1}-\frac{1}{\mathrm{Re}}¢_x^{2}\right)+\Delta^2\left(¢^{-}{}_y\mathbf{Y}\mathbf{\Lambda}^{+}{}_{B}\mathbf{Y}^{-1}+¢^{+}{}_y\mathbf{Y}\mathbf{\Lambda}^{-}{}_{B}\mathbf{Y}^{-1}-\frac{1}{\mathrm{Re}}¢_y^{2}\right)\right]^m\Delta\mathbf{Q}^m$$
$$=\mathbf{S}^m.$$

Finally by suppressing the cross-derivative term which for small Δt will not affect the second-order time accuracy. We thus obtain the AF scheme in the following form

$$\left[\mathbf{I}+\Delta^2\left(¢^{-}{}_x\mathbf{X}\mathbf{\Lambda}^{+}{}_{\mathbf{A}}\mathbf{X}^{-1}+¢^{+}{}_x\mathbf{X}\mathbf{\Lambda}^{-}{}_{\mathbf{A}}\mathbf{X}^{-1}-\frac{1}{\mathrm{Re}}¢_x^{2}\right)\right]\times$$
$$\left[\mathbf{I}+\Delta^2\left(¢^{-}{}_y\mathbf{Y}\mathbf{\Lambda}^{+}{}_{\mathbf{B}}\mathbf{Y}^{-1}+¢^{+}{}_y\mathbf{Y}\mathbf{\Lambda}^{-}{}_{\mathbf{B}}\mathbf{Y}^{-1}-\frac{1}{\mathrm{Re}}¢_y^{2}\right)\right]\Delta\mathbf{Q}^m$$
$$=\mathbf{S}^m. \qquad (11)$$

The system (11) is then solved by the ADI (Alternating Direction Implicit), which is an efficient method as it converges in a number of iterations proportional to the number of points in one direction.

$$\left[\mathbf{I}+\Delta^2\left(¢^{-}{}_x\mathbf{X}\mathbf{\Lambda}^{+}{}_{\mathbf{A}}\mathbf{X}^{-1}+¢^{+}{}_x\mathbf{X}\mathbf{\Lambda}^{-}{}_{\mathbf{A}}\mathbf{X}^{-1}-\frac{1}{\mathrm{Re}}¢_x^{2}\right)\right]\Delta\mathbf{Q}^{**}=\mathbf{S}^m$$
$$\left[\mathbf{I}+\Delta^2\left(¢^{-}{}_y\mathbf{Y}\mathbf{\Lambda}^{+}{}_{\mathbf{B}}\mathbf{Y}^{-1}+¢^{+}{}_y\mathbf{Y}\mathbf{\Lambda}^{-}{}_{\mathbf{B}}\mathbf{Y}^{-1}-\frac{1}{\mathrm{Re}}¢_y^{2}\right)\right]\Delta\mathbf{Q}^{*}=\Delta\mathbf{Q}^{**}$$
$$\Delta\mathbf{Q}^m=\Delta\mathbf{Q}^{*} \qquad (12)$$

Each of these systems of equations is a set of block tri-diagonal equations of the form

$\sim_i\Delta U_{i-1} + \ _i\Delta U_i + ¥_i\Delta U_{i+1} = r_i, \quad i=2,...,\mathrm{imax}-1$ with appropriate boundary conditions.

3. Results and Discussion

As a numerical experiment, a driven cavity flow in a square domain is simulated. The physical configuration consists of a square container filled with incompressible fluid. The upper and lower sides of the container moves at a given, constant velocity in same direction (parallel motion) or in opposite directions (anti parallel motion). The other two walls are at rest. Neuman boundary conditions are used for pressure. The schematics of lid driven cavity for two cases are given in Figure 1.

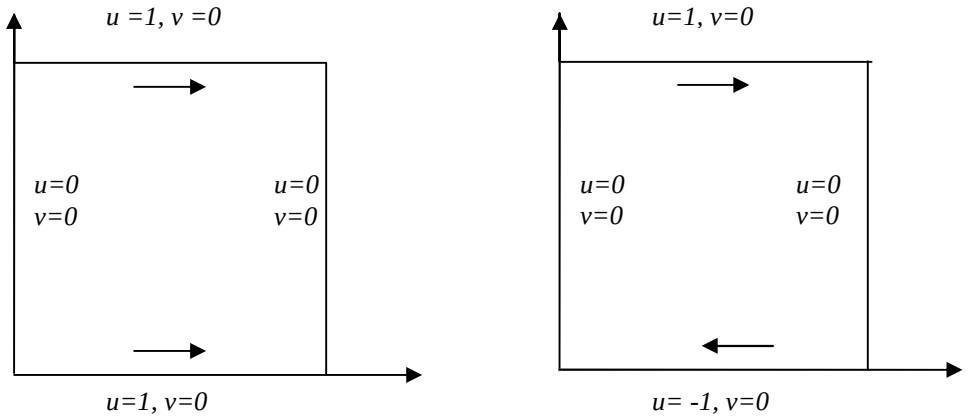

(a) (b)

Figure. 1 Two sided Lid driven square cavity for (a) parallel wall motion (b) anti parallel wall motion.

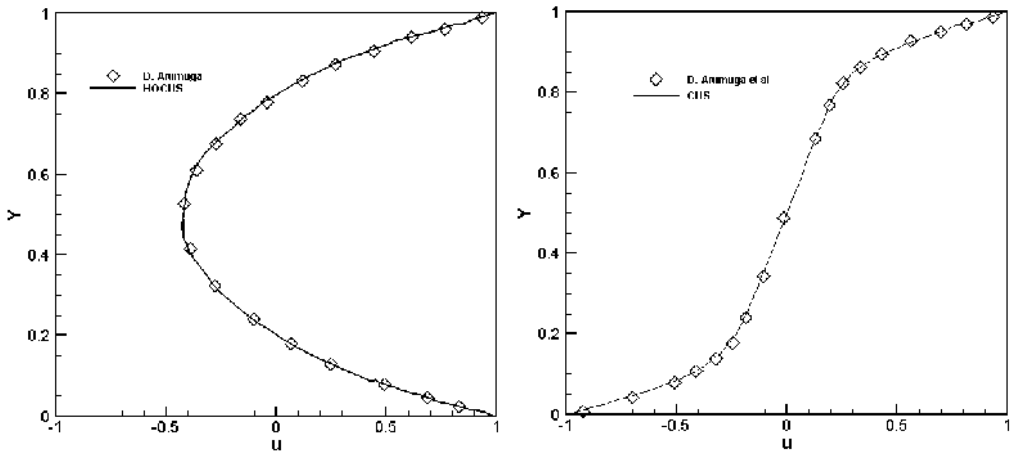

(a) (b)

Fig. 2 Code validation: Horizontal velocity *u* (a) Parallel wall motion (b) Anti parallel wall motion, along the vertical line (x=0.5) for *Re* = 100.

Figures 2(a) and 2(b) shows the steady state x component of velocity along the vertical centre line of square cavity for Reynolds number 100. The results produced by third order compact upwind scheme and finite difference ADI scheme given in [14] are in good agreement. It verifies the accuracy of present computational strategy.

Case I: Parallel Wall Motion

Figure 3 (a-d) shows the flow in a square container, with parallel motion of upper and lower walls with same uniform velocity, the flow field consists of two counter rotating primary eddies, which are symmetrical with respect to the line joining the mid points of side walls. The table 1 elucidates the coordinates of primary eddy centres. These centres shift from right hand top and right hand bottom corners towards the centres of the of top and bottom halves of cavity, with increasing Reynolds number. Moreover, at Reynolds no 400, a pair of secondary counter rotating eddies are seen. These eddies increase in sizes as the Reynolds number is increased beyond 400.

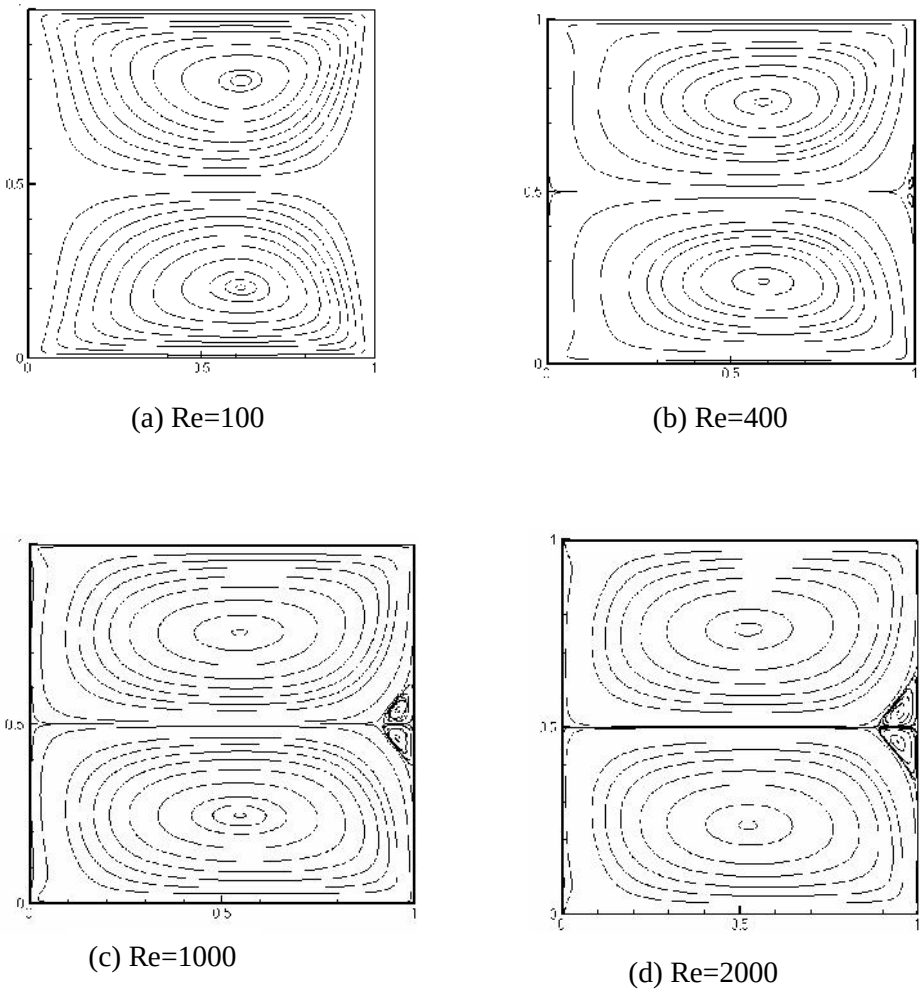

(a) Re=100 (b) Re=400

(c) Re=1000 (d) Re=2000

Figure 3. Steady-state eddy structure for parallel wall motion at (a) *Re* = 100 (b) *Re* = 400 (c) *Re* = 1000 and (d) *Re* = 2000 on a 257 × 257 grid.

TABLE 1: LOCATIONS OF THE EDDIES FOR PARALLEL WALL MOTION USING THIRD ORDER COMPACT UPWIND SCHEME

Re	Primary Eddy Centre				Secondary Eddy Centre			
	Bottom		Top		Bottom		Top	
	x	y	X	y	X	y	x	Y
100	0.61	0.2	0.61	0.8				
400	0.59	0.24	0.59	0.76	0.99	0.46	0.99	0.53
1000	0.54	0.24	0.54	0.76	0.96	0.46	0.96	0.54
2000	0.52	0.24	0.52	0.76	0.94	0.46	0.94	0.54

Case II. Anti-parallel Wall Motion

Figure 4(a-d), shows the eddy structure when upper and lower wall of square cavity are moving in opposite direction with same velocity along the x-axis, for Re=100, 400, 1000 and 2000. A single primary eddy appears for Reynolds number 100 and 400 as shown in Figures 4(a) and 4(b). Two counter rotating secondary eddies appear for Re=1000 and 2000, as clear from Figures 4(c) and 4(d). The size of secondary eddy grows when Re is increased

from 1000 to 2000. These computations were made on grid size 257x257. The location of centres for each primary and secondary eddy is given in Table-2.

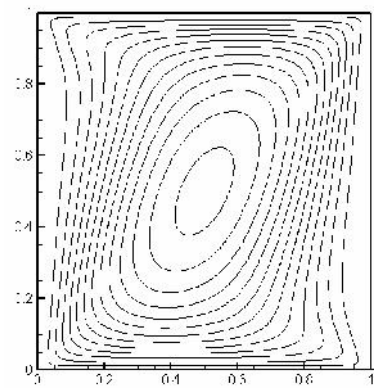

4(a)

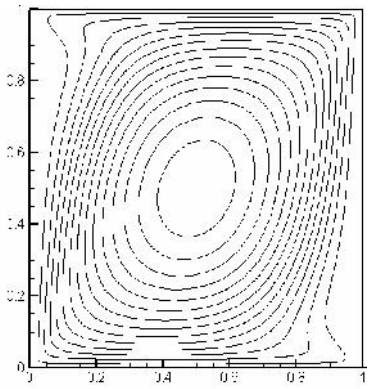

4(b)

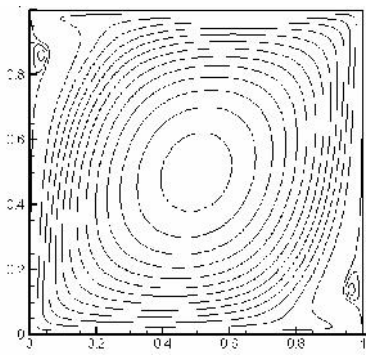

4(c)

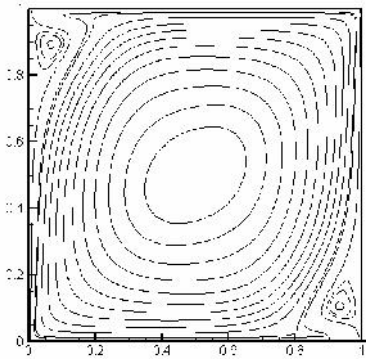

4(d)

Figure 4. Streamline pattern for anti-parallel wall motion at (a) *Re* = 100 (b) *Re* = 400 (c) *Re* = 1000 and (d) *Re* = 2000 on a 257 × 257 grid.

TABLE 2: LOCATIONS OF THE EDDIES FOR ANTI- PARALLEL WALL MOTION USING THIRD ORDER COMPACT UPWIND SCHEME

Re	Primary Eddy Centre		Secondary Eddy Centre			
			Bottom		Top	
	X	Y	x	Y	x	y
100	0.500	0.500	-	-	-	-
400	0.500	0.495	-	-	-	-
1000	0.499	0.500	0.9685	0.1408	0.0338	0.857
2000	0.500	0.500	0.9550	0.111	0.0444	0.887

4. Pressure and Vorticity Fields in the Square Cavity

As the lid moves, the fluid is set into motion due to viscosity of fluid, away from the lid, the fluid is driven by pressure gradient. There is pressure suction near the left side wall and pressure build up on right. Moreover there are also vorticity peaks at same locations. Figure 5 shows these facts in detail.

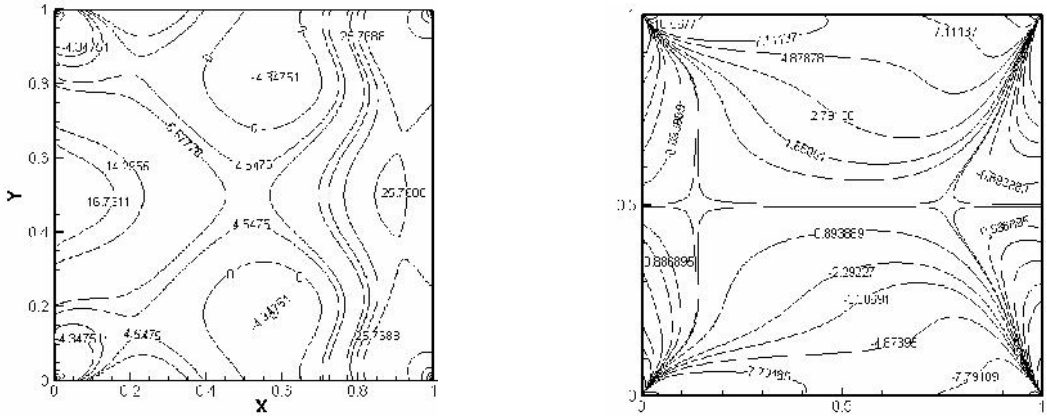

Figure 5. Pressure and vorticity contours for parallel wall motion at *Re* = 100 on 257 × 257 grid.

5. Conclusion

In the present work, flow in two sided lid driven square cavity is observed for parallel and anti parallel motion of top and bottom sides. For parallel motion, there is a free shear layer along the mid line joining the side walls and secondary eddies appear for *Re=400*, which grows in size with decreasing viscosity. Moreover, for anti-parallel wall motion, there is single primary eddy for Reynolds number upto 400, the two secondary eddies, on upper left and lower right corners appear, when the Reynolds number is increased beyond 400. The size of these eddies increases with increasing the Reynolds number. The results given by present scheme are in good agreement with those of finite difference alternate direction implicit (ADI) scheme.

REFERENCES

[1] R. Peyret, *Spectral methods for incompressible viscous flow*. Springer, 2001.

[2] C. Canuto, M.Y. Hussaini, A. Quarteroni, T.A. Zhang, *Spectral methods in fluid dynamics*, Springer, 1988.

[3] R.S. Hirsh, High-order accurate difference solutions of fluid mechanics problems by a compact differencing technique. *J. Comput. Phys.* **19**, 90-109, (1975).

[4] S.K. Lele, Compact finite difference schemes with spectral-like resolution. *J. Comput. Phys.***103**, 16-42 (1992).

[5] D.X. Fu, Y.W. Ma, T. Kobayashi, Nonphysical oscillations in numerical solutions: reason and improvement. *CFD J.* **4**(4), 427-450 (1996).

[6] D.X. Fu, Y.W. Ma, A high order accurate finite difference scheme for complex flow fields. *J.Comput. Phys.* **134**, 1-15 (1997).

[7] A.I. Tlstykh, M.V. Lipavskii, On performance of methods with third and fifth-order compact upwind differencing. *J. Comput. Phys.* **140**, 205-232 (1998).

[8] A., Shah, G., Hong and L., Yuan; A third-order upwind compact scheme on curvilinear meshes for the incompressible Navier-Stokes equations, *Commun. Comput. Phys.* **5**(2-4), 712-729 (2009).

[9] A., Shah, and L., Yuan, Flux difference splitting based upwind compact schemes for incompressible Navier-Stokes equations, *Int. J. Numr. Meth. Fluids*, **61**, 552-568, (2009).

[10] U. Ghia, K.N, Ghia, and C.T. Shin, High resolutions for incompressible flow using Navier-Stokes equations and a multigrid method. *J. Comput. Phys*, **43**, 387-411, (1982).

[11] H.C., Kuhlmann, M. Wanschura, and H.J. Rath, Flow in two-sided lid-driven cavities: non-uniqueness, instability, and cellular structures. *J. Comput. Phys*, **336**, 267-299, 1997.

[12] S., Albensoeder, H.C. Kuhlmann, and H.C, Rath, Multiplicity of steady two-dimensional flows in two-sided lid-driven cavities. *Theoretical computational fluid dynamics*, **14**, 223-241, (2001).

[13] C.H., Blohm and H.C., Kuhlmann, The two-sided lid-driven cavity: experiments on stationary and time-dependent flows. *Journal of Fluid Mechanics*, **450**, 67-95, 2002.

[14] D. Arumuga Perumal and Anoop K. Dass, Simulation of incompressible flows in two-sided lid-driven square cavities. Part I–FDM, *CFD Letters*, **2(1)**, 13-24, (2010)